

Frolov Black Hole Surrounded by Quintessence - II: Quasinormal Modes, Greybody Factors, Deflection Angle and Chaos Bound

Mrinmoy M. Gohain^{1,2,*} Kalyan Bhuyan^{1,3,†} and Hari Prasad Saikia^{1,‡}

¹*Department of Physics, Dibrugarh University, Dibrugarh
Assam, India, 786004*

²*Department of Physics, DHSK College, Dibrugarh
Assam, India, 786001*

³*Theoretical Physics Division, Centre for Atmospheric Studies,
Dibrugarh University, Dibrugarh, Assam, India 786004*

In this work, we have examined the scalar quasinormal modes, greybody factors, weak gravitational lensing, and the chaos bound of a Frolov black hole surrounded by a quintessence field. We studied the quasinormal frequencies and deduced that an increase in the value of the quintessence parameter c dissipates the oscillatory behavior and thus slow down the decay of perturbations. The greybody factors are highly dependent on the multipole moment l and BH parameters, with a larger q hindering the transmission and smaller α_0 making the barrier steeper. The deflection angle of weak lensing under thin lens approximation, monotonically decreases as the value of impact parameter b increases, and is visibly affected by the parameter c , and that α_0 and q has very minimal effect. Lastly, we investigated the chaos bound behaviour of photon trajectories in the near-horizon neighbourhood, which indicates that it is satisfied for bigger circular photon orbits but broken for smaller ones, with high-angular-momentum photons being chaotic. This violation of the bound points towards the role of quintessence in modifying the thermodynamic features of the BH, with possible adjustments to the standard Bekenstein-Hawking entropy.

I. INTRODUCTION

In theoretical and astrophysical contexts, black holes (BHs) are among the most captivating topics that have gained significant attention in recent decades. After the first direct observation of the BH shadow in the very centre of the M87 galaxy [1] by the Event Horizon Telescope (EHT) collaboration, the importance of BH physics has increased dramatically in recent years. From a historical standpoint, Karl Schwarzschild provided the first known solutions to the Einstein field equations. These solutions, which are later recognised as the Schwarzschild BH solution, indicated the feasibility of a spacetime that contains a spherically symmetric, non-rotating, and chargeless body. The Riessner-Nordström BH is another generalisation of the uncharged Schwarzschild BH to a charged one. Other typical BH types are the Kerr-Newman BH, which represents a charged and rotating axisymmetric BH solution, and the Kerr BH, which describes a rotating and uncharged BH solution. Some of the other important intriguing physical characteristics of BHs include quasinormal modes, thermodynamics, and optical characteristics like lensing and shadows.

In both classical and quantum backgrounds, the theory of GR is known to be UV incomplete, meaning that singularities are present. The centre of the well-known BH systems, such as Kerr, Riessner Nordstrom, and Schwarzschild, features curvature singularities. This suggested that if one wants a UV complete theory, Einstein's GR must be modified. Numerous attempts have been made to develop alternative versions of a UV complete theory, but each modification has its own set of issues. For example, adding derivative and higher order curvature terms to the gravitational action results in what are known as "ghost instabilities," where "ghosts" usually refer to unphysical degrees of freedom. In a seminal study published in 2016 [2], V.L. Frolov developed metrics using a number of intuitive assumptions to determine the existence of non-singular BH solutions without changing the theory of GR. By generalising to the charged case, Frolov presented a number of options in his original study, including the modified Hayward solution. The length scale parameter α_0 (denotes by l in his original paper) is related to the critical energy scale μ since $\alpha_0 = \mu^{-1}$. Thus, in addition to the BH's mass, there is another parameter in his own work called α_0 that essentially sets the scale at which the modification of Einstein equations becomes relevant. Technically speaking, at a scale where α_0^{-2} is equivalent to the curvature scalar R . The second argument is that the standard metric tensor $g_{\mu\nu}$ can be used, and that there is

* mrinmoygohain19@gmail.com

† kalyanbhuyan@dibru.ac.in

‡ hariprasadsaikia@dibru.ac.in

a length scale λ at which quantum gravity effects become prominent. The magnitude of length scale is significantly lower than the parameter α_0 . Because of these presumptions, the solution is not singular at $r = 0$. Song et al. [3] recently, examined the quasinormal modes of a Frolov BH under scalar perturbations, and they found that the QNMs were stable with temporal decay behaviour, where by quantum gravity phenomena takes an important part. Additionally, by constraining the BH parameters in relation to the M87* shadow observational data, Kumar et al. examined the shadow and lensing characteristics of a Frolov BH [4].

In the context of BH physics, BHs are often surrounded by matter, such as accretion disks or possibly exotic matter and fields, which can perturb the surrounding spacetime geometry. These resulting perturbations can change the geodesic motion within the BH spacetime; in other words, the geodesic motion contain the information about the nature of these perturbations. Such perturbations, in turn, will lead the BHs to radiate gravitational waves. It is possible to divide loosely into three stages the dynamical evolution, namely inspiral, merger and then followed by ringdown; and among them, the most interesting is the damping oscillations of black holes leading to QNMs. They depend on both the intrinsic parameters—the mass, charge, and angular momentum of the BH and the nature of perturbations, for example, the scalar or electromagnetic field surrounding it. The frequencies of QNMs are complex-valued, and the real part gives the oscillation frequency of the perturbation, while the imaginary part gives the damping rate. Since QNMs are intrinsically linked to the black hole parameters, they are a vital tool for the investigation of the basic properties of black holes.

Whether these perturbations grow or decay will determine the stability of the BH. The perturbations in a black hole spacetime result in oscillations with characteristic frequencies, now called quasi-normal frequencies (QNF). These oscillations are in general termed as quasinormal modes because their growth or decay is controlled by the stability of the black hole. QNMs are of interest in a number of contexts. Within the context of the AdS/CFT correspondence [5], QNMs allow one to study both equilibrium and non-equilibrium properties of strongly coupled thermal gauge theories by using their gravity dual [6]. More precisely, the QNM spectrum of the dual gravitational background corresponds to the poles of retarded correlators in the associated field theory [7, 8]. QNMs are profoundly important in the understanding of the behaviour of astrophysical BHs and gravitational wave (GW) astronomy. The foundational work on the theory of BH perturbation was first

established by Regge and Wheeler [9], who showed that the equations of motion of a perturbed BH can be expressed in the form of Schrödinger equation of quantum mechanics, which then can be solved through various analytical and numerical techniques. Zerilli [10, 11] extended this framework, and later on Vishveshwara [12] analyzed the Schwarzschild metric stability, identifying the QNM features through GW scattering [13]. Chandrasekhar and Detweiler later proved the isospectrality of the Regge-Wheeler and Zerilli potentials and computed Schwarzschild black hole QNMs using the shooting method [14]. Blome and Mashhoon [15] approximated the effective potential with the Eckart potential to analytically calculate QNMs, while Ferrari and Mashhoon [16] used the Pöschl-Teller potential. Leaver utilized numerical methods for QNM computation by following the Continued Fraction Method (CFM) [17–19]. Other approaches, including the Horowitz-Hubeny (HH) method [20] and the Asymptotic Iteration Method (AIM) [21], have also been developed. Comprehensive reviews on QNMs and their applications can be found in [22–24]. In modified gravity and quantum theories, regular black holes have been proposed [25–27], often resulting from gravity’s coupling with nonlinear electrodynamics. QNMs of regular black holes have been analyzed by Flachi and Lemos [28], Toshmatov et al. [29, 30] and others [31–35].

Geodesic motion around black holes includes a whole family of closed and open orbits, depending on their radial position r from the black hole. There are orbits that could be stable or unstable, depending on an effective potential V that the particles feel. Another way of looking at the geodesic stability is through the Lyapunov exponents. The Lyapunov exponents are powerful mathematical tools in the analysis of chaotic dynamics, mainly used for nonlinear systems. Similarly, they can be applied to investigate particle trajectory stability. Mathematically, the Lyapunov exponents λ quantify the average rate of convergence or divergence of nearby geodesics or geodesic congruences. In particular, the principal Lyapunov exponent can be expressed in terms of the second derivative of the potential V evaluated at the extremum of the potential and yields a direct measure of the stability of the orbits. The Lyapunov exponent in BH systems is constrained with an upper bound, known as the “chaos bound” first derived by Maldacena et al. [36]. This bound is expressed as $\lambda \leq \frac{2\pi T}{\hbar}$, where T is the BH temperature. This bound typically indicates the upper limit on the degree of chaos in quantum thermal systems. Maldacena and his team [36], arrived to this result through the formalism of quantum field theory and shock wave analysis near the BH horizon. Some

of the works based on the use of Lyapunov exponents and chaos bound in BH spacetimes can be found in [37–52]

The paper is planned as follows: In the first part, in Section II we briefly discuss the framework of a Frolov BH surrounded by a quintessence field. In Section III, we shall discuss the effect of scalar perturbation on the Frolov BH and determine the QNMs and hence investigate the influence of the quintessence and other model parameters on the QNM frequencies. In Section IV, we discuss the transmission probability of Hawking radiation in terms of greybody factors. In Section V, we study the behaviour of deflection angle of photon rays in the BH spacetime and how the quintessence affects the trajectories. In Section VI, we study the Lyapunov exponent and chaos bound of null geodesics in the vicinity of the Frolov BH and the effect of quintessence on the chaos bound. Finally, in Section VII we conclude the study and discuss the results.

II. FROLOV BLACK HOLE SURROUNDED BY QUINTESSENCE

The Frolov BH is the charged extension of the Hayward BH described by the metric [3]

$$ds^2 = -f(r)dt^2 + f(r)^{-1}dr^2 + r^2d\Omega^2, \quad (1)$$

where

$$f(r) = 1 - \frac{(2Mr - q^2)r^2}{r^4 + (2Mr + q^2)\alpha_0^2}, \quad (2)$$

and $d\Omega^2 = d\theta^2 + \sin^2\theta d\phi^2$. Here M is the ADM mass of the BH. The Frolov BH is associated with the cosmological constant $\Lambda = 3/\alpha_0^2$, where α_0 is known as the Hubble length (length scale parameter) [3, 53], that would serve as a free parameter of the model. The Hubble length display itself as a Universal hair and is restricted by $\alpha_0 \leq \sqrt{16/27}M$. In our analysis, we shall set $M = 1$ for the sake of simplicity. Another free parameter included in the Frolov BH is the charge parameter q , that satisfies the constraint $0 \leq q \leq 1$. Clearly, in the limiting value of $q \rightarrow 0$, the Frolov BH reduces to the Reissner-Nordstrom (ND) BH solution. Also as $\alpha_0 \rightarrow 0$, one obtains the Schwarzschild BH solution.

Kiselev had suggested an interesting possibility that a quintessence field can affect the properties of the BH. The quintessence field follows the relations [54]

$$T_\phi^\phi = T_\theta^\theta = -\frac{1}{2}(3w+1)T_r^r = \frac{1}{2}(3w+1)T_t^t \quad (3)$$

where w indicates the equation of state (EoS) parameter of the quintessence field. In general, the EoS parameter

w for quintessence field falls within the range $-1 < w < -1/3$.

In this work, which is a follow up of our previous work [55], we shall study the QNMs and chaos bound scenario. We shall try to investigate whether the aforementioned aspects are influenced by the presence of the quintessence field and if yes, how do the QNM frequencies are affected by the the quintessence field.

Following the procedure of Kiselev, the effective metric in the presence of quintessence can be obtained by incorporating the term $-c/r^{3w+1}$ into the BH metric, Eq. (2) as:

$$f(r) = 1 - \frac{(2Mr - q^2)r^2}{r^4 + (2Mr + q^2)\alpha_0^2} - \frac{c}{r^{3w+1}}, \quad (4)$$

In the modified lapse function given by Eq. (4). Following this same technique, few of the recent works are carried out are [56–60] (and references therein). In our work, we shall fix the value of the EoS parameter $w = -2/3$. Here, c is a constant that describes a coupling of the quintessence field with our concerned BH system. Physically, this may represent the intensity of the quintessence field, and we shall consider it as a free parameter and see how it plays a role in the behaviour of the QNMs, greybody bounds, deflection angle and chaotic orbits.

III. QUASINORMAL MODES OF A FROLOV BH SURROUNDED BY QUINTESSENCE

In this section, let us discuss the properties of the QNMs of the Frolov BH and how they are governed by the presence of quintessence field. First of all, let us start by studying how the BH system responds to the perturbations to the massless scalar field Φ . The evolution of the scalar field is governed by the Klein-Gordon (KG) equation, which is

$$\nabla_\mu \nabla^\mu \Phi = \frac{1}{\sqrt{-g}} \partial_\nu (g^{\mu\nu} \sqrt{-g} \partial_\mu \Phi) = 0, \quad (5)$$

Since the spacetime is spherically symmetric, we may use the method of separation of variables involving spherical harmonics $Y_{l,m}(\theta, \phi)$, with l and m denoting the angular and azimuthal quantum numbers respectively. Then, the solution for Φ takes the form [61, 62]

$$\Phi(t, r, \theta, \phi) = \sum_{l,m} \exp(-i\omega t) Y_{l,m}(\theta, \phi) \frac{R_l(r)}{r}. \quad (6)$$

This solution renders the KG equation (5) to the form

$$\frac{1}{r^2} \frac{d}{dr} \left[r^2 f(r) \frac{d}{dr} \left(\frac{R(r)}{r} \right) \right] + \left(\frac{\omega^2}{f(r)} - \frac{l(l+1)}{r^2} \right) \frac{R(r)}{r} = 0. \quad (7)$$

The above Eq. (7) can be restructured into the familiar Schrödinger like form:

$$\frac{d^2 R(r_*)}{dr_*^2} + (\omega^2 - V(r_*)) R(r_*) = 0, \quad (8)$$

where $V(r_*)$ is the effective potential given by:

$$V(r_*) = f(r) \frac{l(l+1)}{r^2} + \frac{f(r)f'(r)}{r}, \quad (9)$$

Here, the angular quantum number l can take values 0, 1, 2, ... and r_* denotes the tortoise coordinate, which is related to radial coordinate r through $dr_*/dr = 1/f(r)$. It spans from $-\infty$ at the event horizon to $+\infty$ towards spatial infinity. It is customary to adopt the simplified notation $r_* \rightarrow x$, $R(r_*) \rightarrow \psi(x)$ and $\omega^2 - V(r_*) \rightarrow Q(x)$. The potential $Q(x)$ takes constant values at $x = \pm\infty$, but not necessarily symmetric at both the ends, and attains a maximum value at some point $x = x_0$.

The Eq. (8) has an exact solution when $Q(x)$ is constant. If $Q(x)$ relies on x , then the equation is exactly solvable for some particular forms of $Q(x)$, and hence for $V(r_*)$. In [83], the WKB approximation was used to solve the Schrödinger-like problem (8). The WKB approach is often applicable when the effective potential varies slowly [84].

Conventionally, the formulation of the WKB problem involves obtaining the solutions for incident, reflected, and transmitted amplitudes, with incident and reflected amplitudes being of equal size. In the context of black hole perturbation, the incident amplitude is zero. As a result, reflected and transmitted amplitudes are found to be of the same order of magnitude. This follows that the WKB approximation is applicable given the following condition:

$$\left. \frac{dQ(x)}{dx} \right|_{x=x_0} = 0. \quad (10)$$

If the turning points are too close, the WKB approximation will become inapplicable. The only possible technique is to match the solutions across each turning point simultaneously. Moreover, the potential in between the two turning point is approximated to a parabolic shape [63]. The matching of the solutions in the different regions is done by employing Taylor expansion of the potential about its maximum, x_0 , as can be easily found in any quantum mechanics textbooks [64, 65].

The solution in the region between the turning points can be obtained by expanding $Q(x)$ around the maximum x_0 . As the solution must be continuous, it is possible to obtain the approximate solutions for the two asymptotic regions where $Q(x) \rightarrow \omega$, a constant, at large distances. The matching conditions gives what is usually known as the quasinormal mode (QNM) condition, because it leads to discrete and complex frequencies called quasinormal frequencies. The condition is given by [66, 67]

$$\frac{Q(x_0)}{\sqrt{2Q''(x_0)}} = -i \left(n + \frac{1}{2} \right) \quad (11)$$

Now if one uses the condition (11) in Eq. (8), it leads to

$$\frac{\omega^2 - V(r_0)}{\sqrt{-2V''(r_0)}} = -i \left(n + \frac{1}{2} \right), \quad (12)$$

or

$$\omega^2 = V(r_0) - i \left(n + \frac{1}{2} \right) \sqrt{-2V''(r_0)} \equiv X - iY. \quad (13)$$

where r_0 represents the maxima of the effective potential. Here, we have also designated $X = V(r_0)$ and $Y = \left(n + \frac{1}{2} \right) \sqrt{-2V''(r_0)}$. This leads to the complex quasinormal frequencies given by

$$\begin{aligned} \omega &= \omega_R - i\omega_I; \\ \text{with } \omega_R &= \frac{\sqrt{\sqrt{X^2 + Y^2} + X}}{\sqrt{2}}, \\ \text{and } \omega_I &= \frac{Y}{\sqrt{2}\sqrt{\sqrt{X^2 + Y^2} + X}} \end{aligned} \quad (14)$$

In our work, we follow the first-order WKB approximation. It is also possible to calculate the higher order WKB approximates, which is currently refrained from this analysis for simplicity. Higher order WKB techniques can be found in refs [68–70].

In the Fig. 1, we present the radial evolution of the effective potential V_{eff} for multipole moments $l = 1$ and $l = 2$. Here, as previously stated, we have fixed an EoS parameter $w = -2/3$. We observe the impact of the parameters c , α_0 , and q from the figure as follows:

- **Quintessence parameter c :** With the increase in the value of the quintessence parameter c , the height of the peak of V_{eff} declines for the case $l = 1$ and for $l = 2$ the change in the height of the peak is moderate.
- **Length Scale Parameter α_0 :** The effective potential is seen to be quite insensitive to α_0 values for $l = 1$; but nonetheless, a slight variation in the position of the peak towards increasing values of r

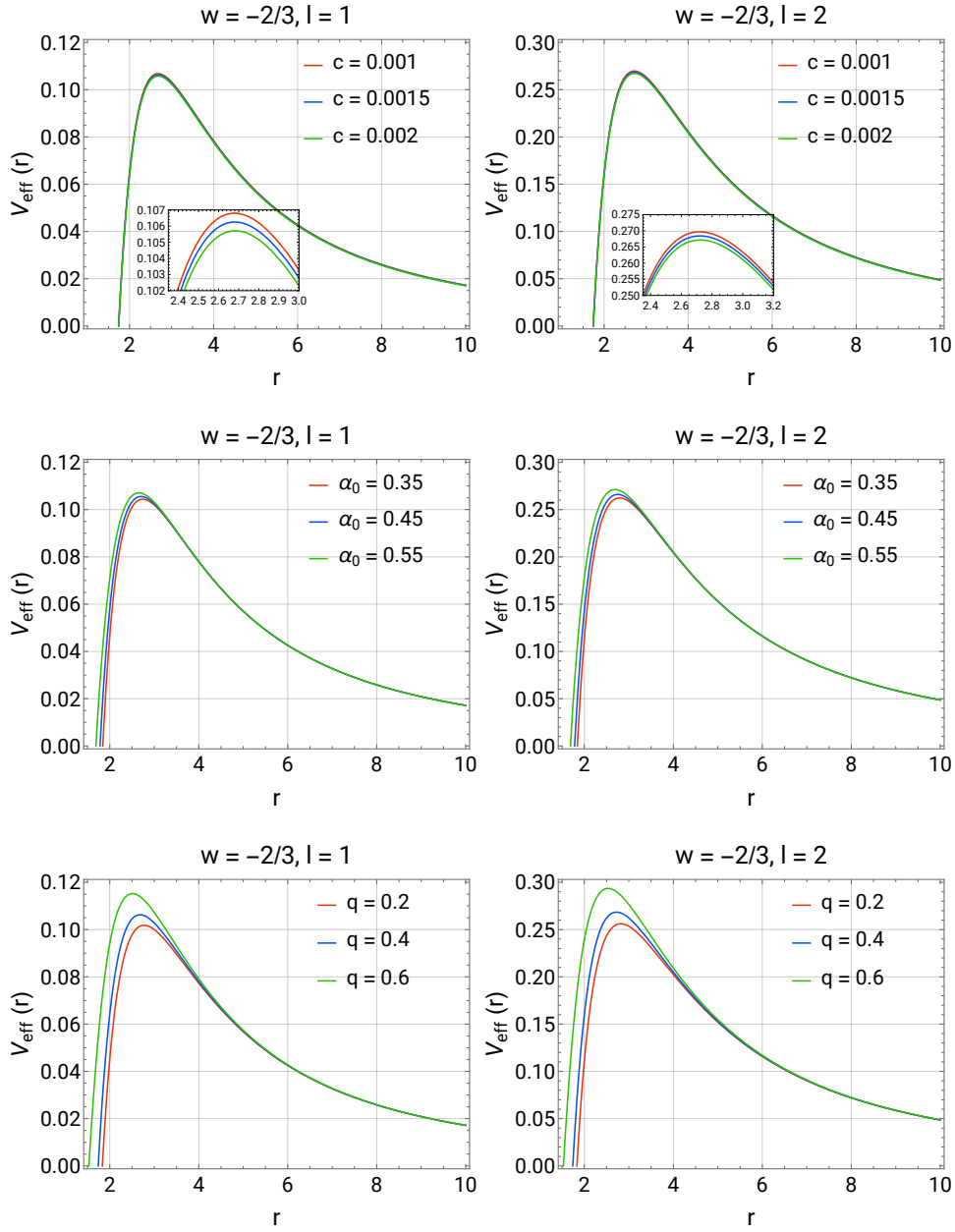


FIG. 1. The plot of the effective potential is shown for different combinations of the parameters c , α_0 and q for $l = 1$ and 2 . In the top panel, α_0 and q are set fixed at 0.5 and 0.4 respectively. In the middle panel, c and q are set at 0.015 and 0.4 and in the bottom panel, c and α_0 are fixed at 0.015 and 0.5 respectively.

is noticed as α_0 decreases. This behaviour is also noticed in the $l = 2$ case, where the height of the peak increases slowly with increasing α_0 .

- **Charge Parameter q :** The peak value of V_{eff} in this case turns out to be highly sensitive to the change in values of q for both $l = 1$ and $l = 2$. For both situations, as q decreases, it reduces the peak value along with shifting the position of the peak towards increasing r values.

The results of the calculated quasinormal modes (QNMs) are presented in Tabs. I, II and III, which show the dependence of the QNM frequencies ω on the parameter c , α and q respectively for a fixed EoS parameter $w = -\frac{2}{3}$. These are also plotted and shown in Figs. 2, 3, 4, 5, 6 and 7. We calculated these QNM frequencies using first order WKB technique for the multipole indices $l = 1$ and $l = 2$ to illustrate how the space-time perturbations evolve in the presence of the Frolov BH in the presence of a quintessence field, with c as

c	$\omega(w = -2/3)$	c	$\omega(w = -2/3)$
0.001	0.415281 - 0.256251 <i>i</i>	0.001	0.586202 - 0.271946 <i>i</i>
0.002	0.413811 - 0.255994 <i>i</i>	0.002	0.583947 - 0.271768 <i>i</i>
0.003	0.412338 - 0.255735 <i>i</i>	0.003	0.581687 - 0.271588 <i>i</i>
0.004	0.410863 - 0.255473 <i>i</i>	0.004	0.579423 - 0.271408 <i>i</i>
0.005	0.409386 - 0.255209 <i>i</i>	0.005	0.577156 - 0.271227 <i>i</i>
0.006	0.407907 - 0.254943 <i>i</i>	0.006	0.574884 - 0.271045 <i>i</i>
0.007	0.406425 - 0.254674 <i>i</i>	0.007	0.572609 - 0.270863 <i>i</i>
0.008	0.404941 - 0.254403 <i>i</i>	0.008	0.570329 - 0.270679 <i>i</i>
0.009	0.403455 - 0.254130 <i>i</i>	0.009	0.568046 - 0.270495 <i>i</i>
0.010	0.401966 - 0.253854 <i>i</i>	0.010	0.565758 - 0.270310 <i>i</i>
0.011	0.400475 - 0.253576 <i>i</i>	0.011	0.563466 - 0.270124 <i>i</i>
0.012	0.398982 - 0.253295 <i>i</i>	0.012	0.561170 - 0.269938 <i>i</i>
0.013	0.397486 - 0.253011 <i>i</i>	0.013	0.558869 - 0.269750 <i>i</i>
0.014	0.395987 - 0.252725 <i>i</i>	0.014	0.556565 - 0.269562 <i>i</i>
0.015	0.394486 - 0.252437 <i>i</i>	0.015	0.554256 - 0.269373 <i>i</i>
0.016	0.392982 - 0.252146 <i>i</i>	0.016	0.551942 - 0.269183 <i>i</i>
0.017	0.391475 - 0.251852 <i>i</i>	0.017	0.549624 - 0.268993 <i>i</i>
0.018	0.389966 - 0.251555 <i>i</i>	0.018	0.547302 - 0.268801 <i>i</i>
0.019	0.388454 - 0.251256 <i>i</i>	0.019	0.544975 - 0.268609 <i>i</i>
0.020	0.386940 - 0.250954 <i>i</i>	0.020	0.542644 - 0.268416 <i>i</i>

TABLE I. Quasinormal mode frequencies ω for different c for $l = 1$ (left) and $l = 2$ (right).

α_0	$\omega(w = -2/3)$	α_0	$\omega(w = -2/3)$
0.010000	0.412891 - 0.260153 <i>i</i>	0.010000	0.576357 - 0.273981 <i>i</i>
0.038421	0.412902 - 0.260136 <i>i</i>	0.038421	0.576402 - 0.273976 <i>i</i>
0.066842	0.412924 - 0.260101 <i>i</i>	0.066842	0.576501 - 0.273964 <i>i</i>
0.095263	0.412959 - 0.260045 <i>i</i>	0.095263	0.576654 - 0.273946 <i>i</i>
0.123684	0.413006 - 0.259969 <i>i</i>	0.123684	0.576861 - 0.273921 <i>i</i>
0.152105	0.413065 - 0.259872 <i>i</i>	0.152105	0.577122 - 0.273887 <i>i</i>
0.180526	0.413136 - 0.259753 <i>i</i>	0.180526	0.577438 - 0.273844 <i>i</i>
0.208947	0.413217 - 0.259611 <i>i</i>	0.208947	0.577810 - 0.273791 <i>i</i>
0.237368	0.413310 - 0.259443 <i>i</i>	0.237368	0.578239 - 0.273724 <i>i</i>
0.265789	0.413414 - 0.259247 <i>i</i>	0.265789	0.578725 - 0.273644 <i>i</i>
0.294211	0.413528 - 0.259022 <i>i</i>	0.294211	0.579270 - 0.273545 <i>i</i>
0.322632	0.413651 - 0.258765 <i>i</i>	0.322632	0.579874 - 0.273426 <i>i</i>
0.351053	0.413782 - 0.258471 <i>i</i>	0.351053	0.580539 - 0.273282 <i>i</i>
0.379474	0.413921 - 0.258136 <i>i</i>	0.379474	0.581267 - 0.273108 <i>i</i>
0.407895	0.414065 - 0.257756 <i>i</i>	0.407895	0.582058 - 0.272897 <i>i</i>
0.436316	0.414213 - 0.257324 <i>i</i>	0.436316	0.582914 - 0.272643 <i>i</i>
0.464737	0.414363 - 0.256832 <i>i</i>	0.464737	0.583837 - 0.272334 <i>i</i>
0.493158	0.414511 - 0.256270 <i>i</i>	0.493158	0.584827 - 0.271959 <i>i</i>
0.521579	0.414653 - 0.255627 <i>i</i>	0.521579	0.585885 - 0.271501 <i>i</i>
0.550000	0.414784 - 0.254887 <i>i</i>	0.550000	0.587011 - 0.270940 <i>i</i>

TABLE II. Quasinormal mode frequencies ω for different α_0 for $l = 1$ (left) and $l = 2$ (right).

the intensity of the field. The real part of the QNM frequency, $\text{Re}(\omega)$, that defines the oscillation frequency of the perturbations, is found to decrease monotonically as the value of c increases. This behaviour means that as the intensity of the quintessence field increases, the oscillation frequency of the perturbations becomes progressively smaller, thereby leading to a weaker response

of the BH spacetime. Whereas in contrast, the imaginary part $\text{Im}(\omega)$, that is related to the dissipative rate of the oscillations, becomes less negative with increasing values of c . This indicates that a higher intensity of the quintessence field leads to a slower dissipation rate of the perturbations, which implies that the oscillations sustain for a longer period of time. Such a behaviour can

q	$\omega(w = -2/3)$	q	$\omega(w = -2/3)$
0.010000	0.412891 - 0.260153i	0.010000	0.576357 - 0.273981i
0.038421	0.412902 - 0.260136i	0.038421	0.576402 - 0.273976i
0.066842	0.412924 - 0.260101i	0.066842	0.576501 - 0.273964i
0.095263	0.412959 - 0.260045i	0.095263	0.576654 - 0.273946i
0.123684	0.413006 - 0.259969i	0.123684	0.576861 - 0.273921i
0.152105	0.413065 - 0.259872i	0.152105	0.577122 - 0.273887i
0.180526	0.413136 - 0.259753i	0.180526	0.577438 - 0.273844i
0.208947	0.413217 - 0.259611i	0.208947	0.577810 - 0.273791i
0.237368	0.413310 - 0.259443i	0.237368	0.578239 - 0.273724i
0.265789	0.413414 - 0.259247i	0.265789	0.578725 - 0.273644i
0.294211	0.413528 - 0.259022i	0.294211	0.579270 - 0.273545i
0.322632	0.413651 - 0.258765i	0.322632	0.579874 - 0.273426i
0.351053	0.413782 - 0.258471i	0.351053	0.580539 - 0.273282i
0.379474	0.413921 - 0.258136i	0.379474	0.581267 - 0.273108i
0.407895	0.414065 - 0.257756i	0.407895	0.582058 - 0.272897i
0.436316	0.414213 - 0.257324i	0.436316	0.582914 - 0.272643i
0.464737	0.414363 - 0.256832i	0.464737	0.583837 - 0.272334i
0.493158	0.414511 - 0.256270i	0.493158	0.584827 - 0.271959i
0.521579	0.414653 - 0.255627i	0.521579	0.585885 - 0.271501i
0.550000	0.414784 - 0.254887i	0.550000	0.587011 - 0.270940i

TABLE III. Quasinormal mode frequencies ω for different q and $w = -2/3$ for $l = 1$ (left) and $l = 2$ (right).

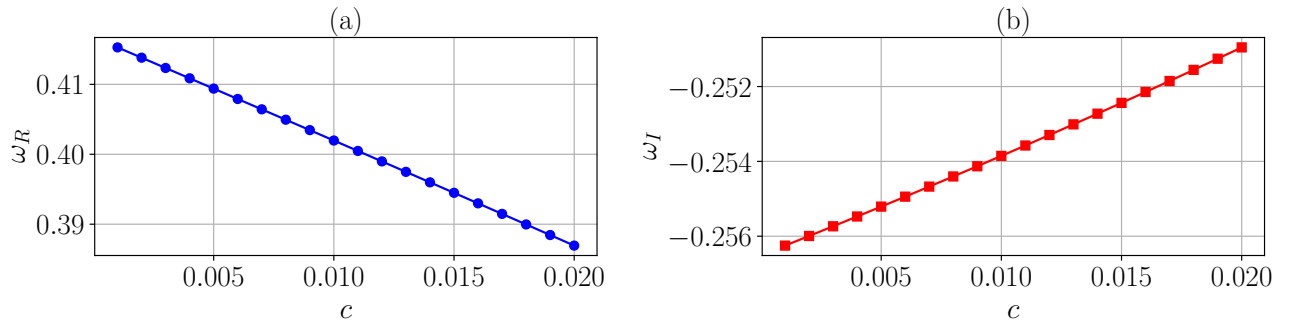


FIG. 2. Plot of real and imaginary components for $w = -2/3$ and $n = 0$, $l = 1$, $\alpha_0 = 0.5$ and $q = 0.4$.

be attributed to the enhanced effect of the quintessence field on the effective potential, which in turn affects the propagation and decay properties of the perturbations.

Furthermore, the QNM frequencies as a function of the length scale parameter α_0 and the charge q are also analyzed. It is observed that $\text{Re}(\omega)$ increases with increasing values of α_0 , which leads to a higher oscillation frequency and thus suggests improved stability of the oscillations for larger values of α_0 . In the meanwhile, as $\text{Im}(\omega)$ becomes more negative, with increasing α_0 values, implies a slower dissipation of the perturbations and more an extended oscillatory behavior. In contrast, the effect of the charge q on the QNM frequencies is opposite to that of α_0 ; as q increases, $\text{Re}(\omega)$ also increases, signifying that the system oscillates faster. Simultaneously, $\text{Im}(\omega)$ becomes less negative with higher

q , meaning that the perturbations decay more slowly. Loosely speaking, the electromagnetic field coupled to the charge parameter in a way “tightens” the effective potential around the BH, thus increasing the oscillatory response and prolongs the time of the oscillations.

In general, the monotonic decrease of the real and imaginary parts of ω with increasing c suggests that a strong quintessence field results in smaller oscillation frequencies and longer-lasting perturbations. The combination of c , α_0 , and q determines the stability and dissipative behaviour of the BH perturbations, which justifies the usefulness of QNM frequencies as sensitive methods for investigating the role of electromagnetic interactions in the physics of BH spacetimes.

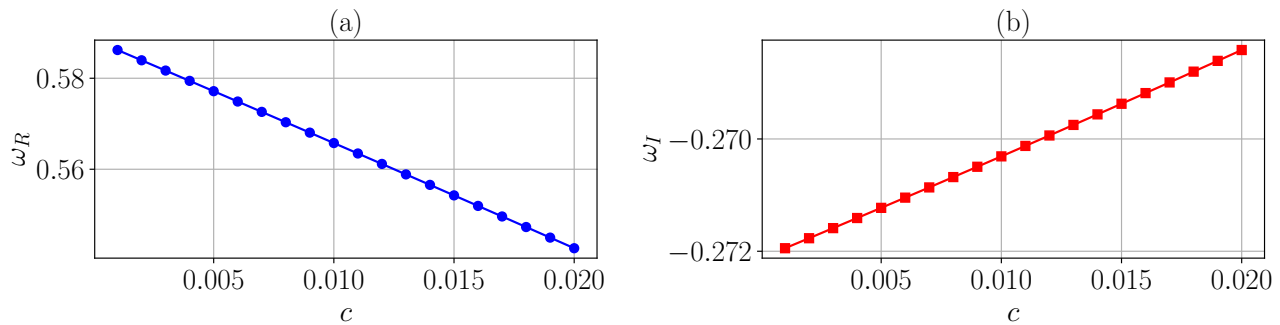


FIG. 3. Plot of real and imaginary components for $w = -2/3$ and $n = 0$, $l = 2$, $\alpha_0 = 0.5$ and $q = 0.4$.

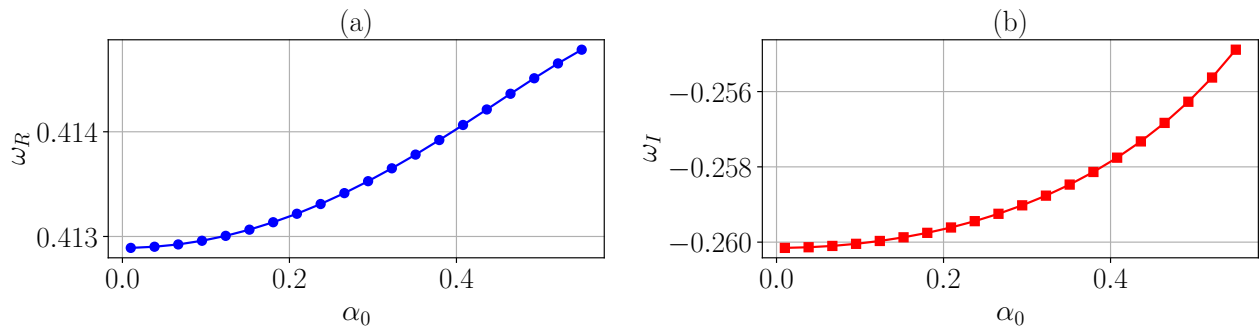


FIG. 4. Plot of real and imaginary components for $w = -2/3$ and $n = 0$, $l = 1$, $c = 0.0015$ and $q = 0.4$.

IV. GREYBODY FACTORS

Hawking proved that a BH can emit thermal radiation at its event horizon such that it is nearly a blackbody spectrum, when quantum effects are taken into consideration. This radiation was later termed as Hawking radiation [71] which interacts with the spacetime curvature around the BH as it departs from the BH, thereby modifying its properties. So, the usual blackbody spectrum of the Hawking radiation cannot be detected by an observer located at infinity. Instead, a rescaled spectrum called the greybody spectrum is observed [72–75]. A measure of the deviation between the rescaled spectrum and the blackbody spectrum is given by the greybody factor. From another perspective, greybody factor is actually a transmission coefficient in black hole scattering, where the curvature of spacetime plays the role of a potential barrier.

By inspection of the Schrödinger-like equation (cf. Eq. (8)), the potential $V(r)$ clearly acts as a barrier that filters the propagation of the scalar field in the black hole spacetime. In this context, part of the field passes through the potential barrier while the rest is reflected, which modulates the properties of Hawking radiation and any other fields moving through this curved back-

ground. Since the potential $V(r)$ is determined only by the geometry of spacetime, its function in filtering the radiation directly stems from the gravitational structure. The greybody factor, which is qualitatively identical to the absorption cross section σ_{abs} of a black hole, indicates how much of the incoming field penetrates the barrier and is subsequently absorbed. In consequence, the radiation spectrum of the black hole is not exactly similar to that of a perfect black body; rather, it effectively resembles a grey body spectrum. This change in the spectral profile led to the term “greybody factor,” which emphasizes the interrelationship of quantum mechanical tunneling phenomenon to the intrinsic geometry of the BH spacetime. An illustration of the formation of a greybody region is shown in Fig. 8.

There are several methods to compute the greybody factor. One of such methods is to find its lower bound instead its exact value, which can be termed as *greybody bound*. We specifically follow the method given by Visser and Boonserm [76, 77], where the greybody bound is given by

$$T_b \geq \text{sech}^2 \left(\frac{1}{2\omega} \int_{r_h}^{\infty} |V| \frac{dr}{f(r)} \right) \quad (15)$$

where r_h is the horizon radius.

To see how the greybody bounds depends on l , it

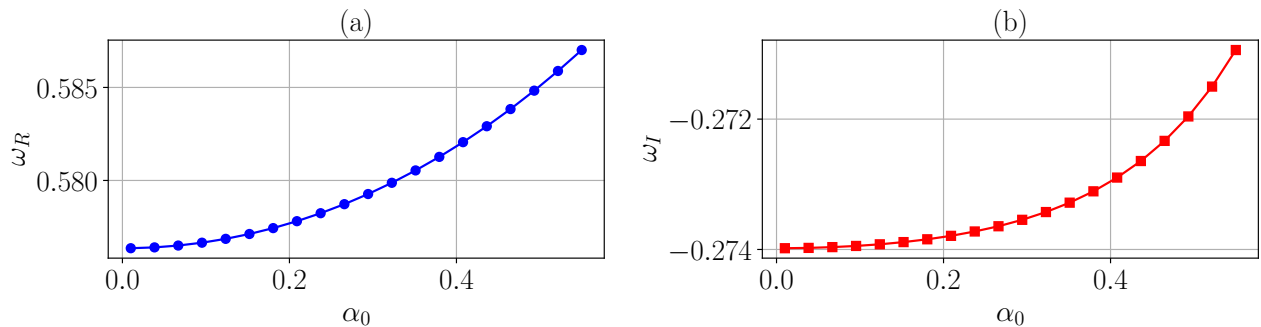


FIG. 5. Plot of real and imaginary components for $w = -2/3$ and $n = 0$, $l = 2$, $c = 0.0015$ and $q = 0.4$.

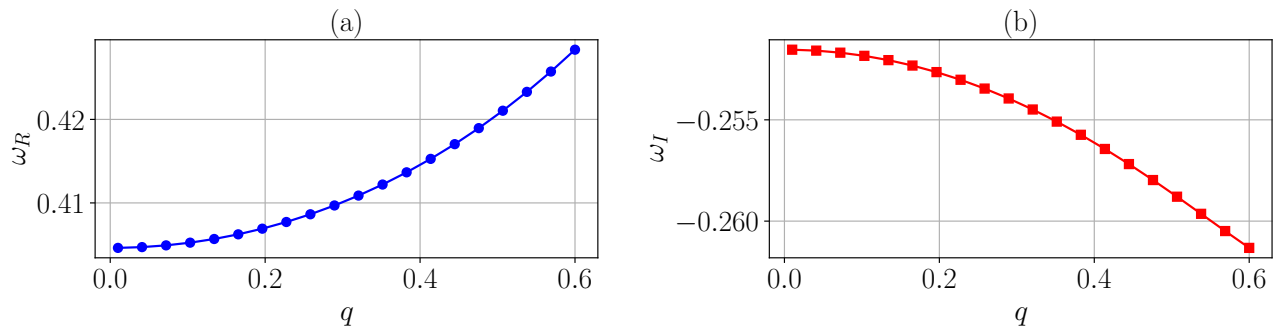


FIG. 6. Plot of real and imaginary components for $w = -2/3$ and $n = 0$, $l = 1$, $\alpha_0 = 0.5$ and $c = 0.0015$

is found that for lower multipole moment modes, $l = 1$, the transmission coefficient rises more quickly with frequency, suggesting that these modes experience a weaker effective potential barrier and thus have a higher chance of escaping. But, for higher values $l = 2$, the greybody factor consistently remains lower for all frequencies, which indicating that higher l modes experience stronger centrifugal repulsion, which increases reflection and decreases transmission efficiency. This pattern arises from the modified Regge-Wheeler potential, where a rise in l results in a greater height of the effective potential barrier, thus preventing the transmission of lower-energy waves.

The greybody factors of the Frolov BH is also influenced by additional BH parameters, such as the charge q , the Hubble length α_0 , and the quintessence parameter c . The presence of an electric charge modifies the effective potential, typically increasing its height and leading to stronger reflection, thereby reducing the transmission probability, particularly at intermediate frequencies. The quintessence field, parameterized by c , introduces an additional effect in the metric, which influences the effective potential in a manner dependent on the EoS of the surrounding field. A higher value of c generally modifies the location and reduces the height of the barrier potential, thereby improving the transmis-

sion of the low-energy modes. This is one of the results in this study. Nevertheless, variations in the choice of the c parameter in this work, does not drastically lead to observable shifts in the greybody profile. The Hubble length parameter α_0 , affects the potential barrier structure, thus modifying the transmission of the waves. As the value of α_0 decreases, the height of the slope becomes steeper, which indicates an increased intensity of opposition to the transmission of the waves. The dependency on α is however found to be very weak, but noticeable for both $l = 1$ and $l = 2$ cases.

Additionally, the behavior of T_b in response to the charge q is seen to be quite prominent. That is, as the charge parameter increases, the slope of the curve also increases. This suggests that as q increases, the resistance to transmission of outgoing waves also rises. This behaviour is further amplified as l is increased from 1 to 2.

V. WEAK LENSING

In this section, we shall calculate the weak deflection angle of light around the Frolov black hole, assuming the presence of a quintessence field. The intention of investigating the weak deflection angle is to figure out the

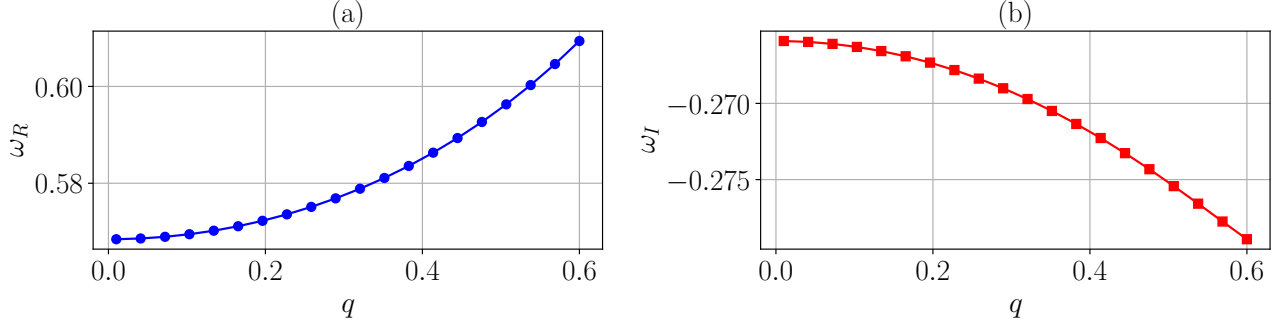


FIG. 7. Plot of real and imaginary components for $w = -2/3$ and $n = 0$, $l = 2$, $\alpha_0 = 0.5$ and $c = 0.0015$.

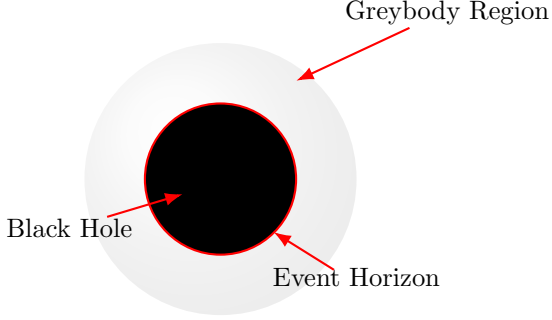


FIG. 8. An illustration of greybody region around a BH is shown. Greybody factors, as one can see, are named for the way they modify the BH's spectrum, transforming it from that of a 'black-body' to that of a 'grey-body'.

effect of quintessence and other associated Frolov BH parameters on the trajectory of light beams. In case of weak lensing, the light source and receiver are placed at finite radial distances $r = r_S$ and $r = r_R$ from the black hole, respectively (see Fig. 11). In such a picture, the deflection angle can be defined as follows [78]:

$$\alpha \equiv \Psi_R - \Psi_S - \phi_{RS} \quad (16)$$

where Ψ_R and Ψ_S are the angles between the direction of light propagation and the radial direction at the receiver's position (R) and the source's position (S), respectively. The term ϕ_{RS} denotes the change in the azimuthal angle ϕ arising due to bending of light rays. Now, for a spherically symmetric spacetime, the metric in Eq. (1), the angle between the direction of light

propagation and the radial direction is determined by [78, 79]:

$$\sin \Psi = \frac{b \cdot \sqrt{f(r)}}{r} \quad (17)$$

Under the thin lens approximation, this definition of the gravitational deflection angle, applicable for finite source and observer distances, is illustrated in Fig. 11. In the figure, S and R denotes the coordinates of the source and receiver and Ψ_R and Ψ_S are the angles between the direction of propagation of light and the radial directions at the receiver's position (R) and the source's position (S), respectively. In the thin lens approximation, the deflection angle $\alpha \equiv \Psi_R - \Psi_S - \Delta\phi_{RS}$ can be demonstrated through the quadrilateral. The exterior angles at each vertex of the quadrilateral are Ψ_S , α , $\pi - \Psi_O$, and $\pi - \Delta\phi_{RS}$, respectively. In this approximation one can assume that the spacetime is flat everywhere except at the thin lens position (the central black hole). As a result, the sum of the exterior angles equals 2π , which explains the definition of the deflection angle $\alpha \equiv \Psi_R - \Psi_S - \Delta\phi_{RS}$.

In spherically symmetric spacetimes, the angle ϕ_{RS} can be derived from the geodesic equation

$$\frac{dr}{d\phi} = \frac{dr}{d\lambda} \cdot \frac{d\lambda}{d\phi} = \pm r^2 \sqrt{\frac{1}{b^2} - \frac{f(r)}{r^2}} \quad (18)$$

where λ is the affine parameter, and $\epsilon = 0$ for null rays. It is straightforward that the conserved quantities are the energy $E = f(r) \frac{dt}{d\lambda} = f(r) \dot{t}$, and the angular momentum $L = r^2 \sin^2 \theta \frac{d\phi}{d\lambda} = r^2 \sin^2 \theta \dot{\phi}$, which can be used to define the impact parameter through $b = |L/E|$.

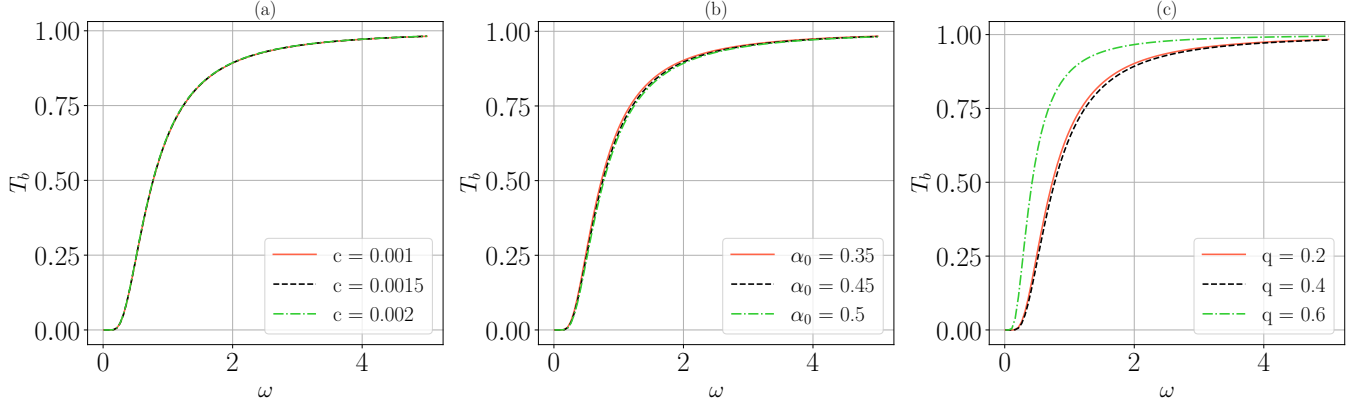


FIG. 9. Greybody bounds for different choices of c , α_0 and q for $w = -2/3$ and $l = 1$

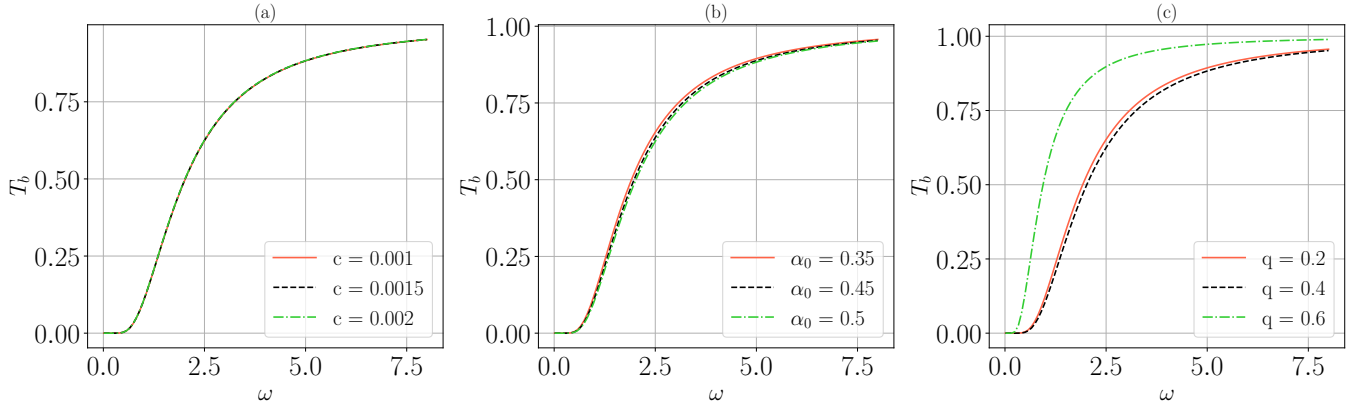


FIG. 10. Greybody factor for different choices of c , α_0 and q for $w = -2/3$ and $l = 2$

$$\left. \begin{aligned} \frac{dr}{d\phi} = -r^2 \sqrt{\frac{1}{b^2} - \frac{f(r)}{r^2}} < 0 \\ \frac{dr}{d\phi} = r^2 \sqrt{\frac{1}{b^2} - \frac{f(r)}{r^2}} > 0 \end{aligned} \right\} \begin{aligned} &\text{photon going from } S(r = r_S) \text{ to the closest approach point } r = r_0 \\ &\text{photon going from the closest approach point } r = r_0 \text{ to } R(r = r_R) \end{aligned}$$

Now using the angle Ψ from Eq. (17) and the angle ϕ_{RS} , the weak deflection angle of can be expressed in a

general form as [79]

$$\begin{aligned} \alpha &= \Psi_R - \Psi_S - \Delta\phi_{RS} = \Psi_R - \Psi_S + \int_{r_S}^{r_0} \frac{d\phi}{dr} dr + \int_{r_0}^{r_R} \frac{d\phi}{dr} dr \\ &= \arcsin\left(\frac{b\sqrt{f(r_R)}}{r_R}\right) + \arcsin\left(\frac{b\sqrt{f(r_S)}}{r_S}\right) - \pi + \int_{r_0}^{r_S} \frac{dr}{r^2 \sqrt{\frac{1}{b^2} - \frac{f(r)}{r^2}}} + \int_{r_0}^{r_R} \frac{dr}{r^2 \sqrt{\frac{1}{b^2} - \frac{f(r)}{r^2}}} \end{aligned} \quad (20)$$

Like shown in Fig. 11, the angle Ψ at the coordinate of

light source S is an obtuse angle given by $\Psi_S = \pi -$

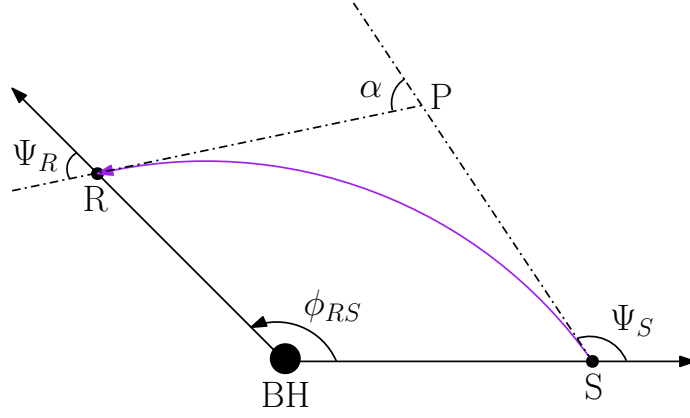


FIG. 11. An illustration of the deflection angle of light trajectories around the BH is shown.

$$\arcsin\left(\frac{b\sqrt{f(r_s)}}{r_s}\right).$$

With the help of Eq. (20), the deflection angle α is solved numerically and plotted against the impact parameter b for different combinations of the model parameters c , α_0 , and q . The results are shown in Fig. 12(i)–(iii). As seen from Fig. (12)(i), the deflection angle decreases monotonically with a larger impact parameter b . For this case, we choose three different values of c , whereas α_0 and q are fixed at 0.5 and 0.4, respectively. As can be observed, a mild variation in the deflection angle is apparent for larger values of b , with greater c values corresponding to an increased rate of decrease in α . A higher c parameter, associated with the density or spatial distribution of quintessence, might enhance its repulsive gravitational influence at larger distances and thus decrease light-bending even more as b increases. Contrastingly, in Fig. 12 (ii) and (ii), where $(c, q) = (0.0015, 0.4)$ and $(c, \alpha_0) = (0.0015, 0.5)$ are kept fixed respectively, the variation in the deflection angle is quite insensitive to the parameters α_0 and q , as no noticeable variation in α is seen.

VI. CHAOTIC BEHAVIOUR: LYAPUNOV EXPONENTS

The Lyapunov exponent is the average rate at which two neighbouring geodesics separation within phase plane. If the Lyapunov exponent is positive, these geodesics are said to diverge, while if it is negative, then they are said to converge. The fact that BH spacetimes have unstable circular geodesics also shows us that GR is non-linear, which reflects on a positive Lyapunov exponent. This non-linearity suggests that the system is not integrable but the circular geodesics can behave chaotically as a consequence.

The Lyapunov exponent ($\tilde{\lambda}$) is directly related to the

effective potential through the relation [52]

$$\tilde{\lambda}^2 = -\frac{(V_{eff})''}{2\dot{t}^2}, \quad (21)$$

where $\dot{t} = Ef(r)^{-1}$ and $V_{eff} = f(r)\left(\frac{E^2}{f(r)} + \frac{L^2}{2r^2}\right)$ are the derivative of the coordinate t with respect to a affine parameter (say μ) and V_{eff} is the effective potential for massless particles respectively. Also, $(\prime\prime)$ represents the second derivative with respect to r . In the subsequent analysis, we can safely set $E = 1$ for simplicity. The value of E is only responsible for the height of the peak of the effective potential, and does not affect the radius of the circular orbits.

The circular geodesics are said to be unstable, stable and marginally stable if the Lyapunov exponent $\tilde{\lambda}$ attains real, imaginary and zero values. In our model, we calculate the Lyapunov exponent as

$$\begin{aligned} \tilde{\lambda}^2 = & \frac{1}{4E^2 (2\alpha_0^2 M r_c + r_c^4 + \alpha_0^2 q^2)^5} \\ & \times [L^2 r_c^{-9w-7} (c (2\alpha_0^2 M r_c + r_c^4 + \alpha_0^2 q^2) \\ & - r_c^{3w+1} (2\alpha_0^2 M r_c - 2M r_c^3 + q^2 (\alpha_0^2 + r_c^2) + r_c^4))^2 \\ & \times \left(3c (3w^2 + 7w + 4) (2\alpha_0^2 M r_c + r_c^4 + \alpha_0^2 q^2)^3 \right. \\ & - 2r_c^{3w+1} \left(q^2 r_c^2 (8\alpha_0^4 M^2 r_c^2 + 24\alpha_0^2 M r_c^5 + 36\alpha_0^4 M r_c^3 \right. \\ & + 9\alpha_0^2 r_c^6 + 10r_c^8 + 36\alpha_0^6 M^2) \\ & + 3r_c^3 (4\alpha_0^2 M^2 r_c^3 (3\alpha_0^2 + r_c^2) + M (6\alpha_0^2 r_c^6 - 4r_c^8) \\ & + r_c^9 + 8\alpha_0^6 M^3) \\ & \left. \left. + q^4 (18\alpha_0^6 M r_c - 6\alpha_0^2 r_c^6 + 9\alpha_0^4 r_c^4) + 3\alpha_0^6 q^6 \right) \right]. \end{aligned} \quad (22)$$

The behavior of the squared Lyapunov exponent $\tilde{\lambda}^2$ as a function of circular orbit radius r_c is dictated by

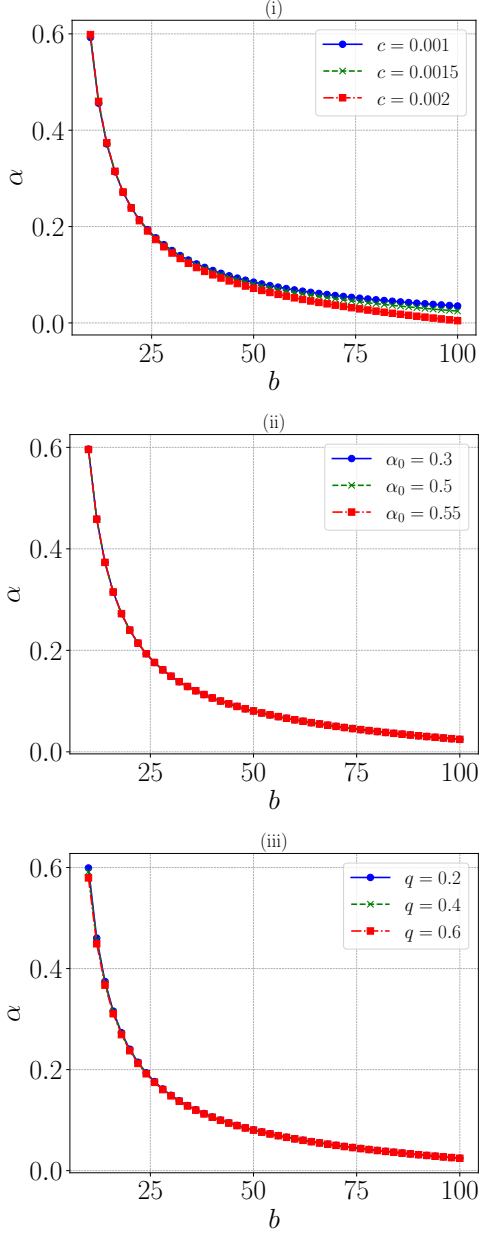


FIG. 12. The weak deflection angle is plotted against the impact parameter for three values of c , α_0 and q . In the plots (i), (ii) and (iii), $(\alpha_0, q) = (0.5, 0.4)$, $(c, q) = (0.0015, 0.4)$ and $(\alpha_0, c) = (0.5, 0.0015)$ are kept fixed respectively.

the requirement $\dot{r} = 0$. In Fig. 13, one can see that for

smaller radii of r_c , λ^2 is positive, showing that the circular photon orbits are unstable because the nearby trajectories experience exponential divergence. For large values of radii, however, λ^2 becomes negative, which marks a marginally stable regime. Additionally, the figures suggest that as angular momentum L is increased, λ^2 also increases monotonically, that emphasizes the correspondence of orbital instability with angular momentum within the black hole spacetimes.

Here, the vertical axis measures the square Lyapunov exponent λ^2 , quantitatively computing the stability of circular orbits of photons for black holes. All the panels show λ^2 vs. either the orbit radius r_c (left column) or the angular momentum of the photon L (right column) with the quintessence parameter c , the length scale α_0 , and the black hole charge q varied systematically. A positive values of $\tilde{\lambda}^2$ means that small perturbations in the trajectory of the photon will grow exponentially, which a signifies dynamical instability, while a negative value of $\tilde{\lambda}^2$ signifies a stable or marginally stable photon orbit.

To predict the existence of chaotic behaviour, one can calculate the chaos bound of the null circular geodesics. Chaos is an interesting phenomenon observed in non-linear physical systems, which represents unpredictable random motion in some deterministic but non-linear systems sourcing from the susceptibility to the initial conditions. It is known for a general chaotic system, that if chaos is mathematically expressed as a function of time $C(t)$, it grows exponentially over time, i.e. $C(t) \approx \exp(\tilde{\lambda}t)$, where $\tilde{\lambda}$ is called the Lyapunov exponent, which manifests as the system's sensitivity to the initial conditions. Maldacena, Shenker and Stanford had proposed a conjecture that there should exist a universal upper bound for the Lyapunov exponent in general BH thermodynamic systems [36], i.e.

$$\tilde{\lambda} \leq \frac{\kappa}{\hbar}, \quad (23)$$

where κ represents the surface gravity of the BH which is associated with the temperature of the BH through $T = \kappa/2\pi$. This is known as the chaos bound. Since, the BH surface gravity κ is defined as $\kappa = f'(r)/2$, it is straight forward to calculate $\tilde{\lambda}^2 - \kappa^2$ and considering units where $\hbar = 1$, this gives

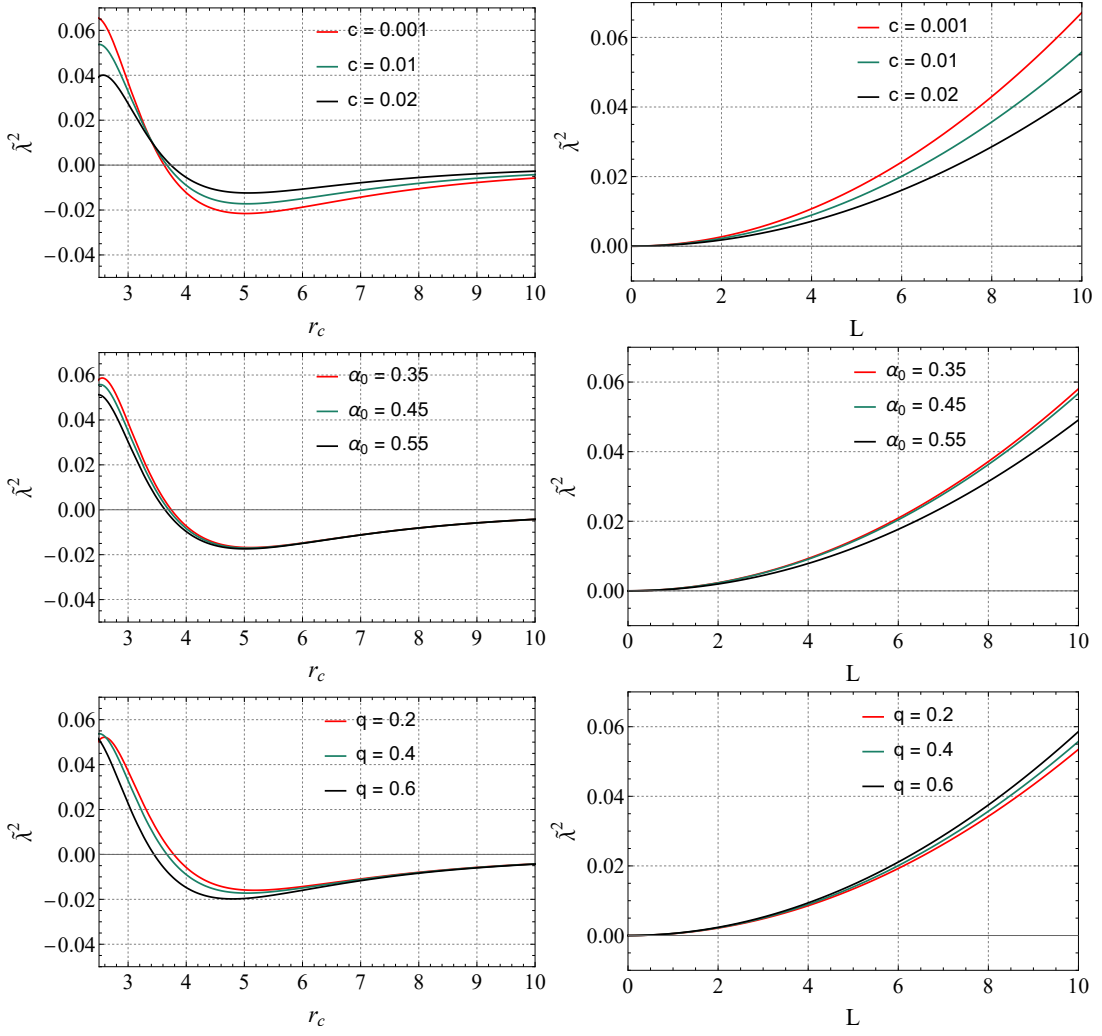


FIG. 13. The Lyapunov exponent $\tilde{\lambda}^2$ is plotted with respect to r_c and L for different values of c (top panel), α_0 (middle panel) and q (bottom panel).

$$\begin{aligned}
\tilde{\lambda}^2 - \kappa^2 = & \frac{1}{4(2\alpha_0^2 M r_c + r_c^4 + \alpha_0^2 q^2)^5} \times \left[\right. \\
& r_c^{-9w-7} \left(\frac{L^2 \left(c(2\alpha_0^2 M r_c + r_c^4 + \alpha_0^2 q^2) - r_c^{3w+1} (2\alpha_0^2 M r_c - 2M r_c^3 + q^2(\alpha_0^2 + r_c^2) + r_c^4) \right)^2}{E^2} \right) \\
& \times \left(3c(3w^2 + 7w + 4)(2\alpha_0^2 M r_c + r_c^4 + \alpha_0^2 q^2)^3 - 2r_c^{3w+1} \left(q^2 r_c^2 (8\alpha_0^4 M^2 r_c^2 + 24\alpha_0^2 M r_c^5 + 36\alpha_0^4 M r_c^3 \right. \right. \\
& + 9\alpha_0^2 r_c^6 + 10r_c^8 + 36\alpha_0^6 M^2) + 3r_c^3 (4\alpha_0^2 M^2 r_c^3 (3\alpha_0^2 + r_c^2) + M(6\alpha_0^2 r_c^6 - 4r_c^8) + r_c^9 + 8\alpha_0^6 M^3) \\
& \left. \left. + q^4 (18\alpha_0^6 M r_c - 6\alpha_0^2 r_c^6 + 9\alpha_0^4 r_c^4) + 3\alpha_0^6 q^6 \right) \right) \\
& - r_c^{3w+3} (2\alpha_0^2 M r_c + r_c^4 + \alpha_0^2 q^2) \left(c(3w+1)(2\alpha_0^2 M r_c + r_c^4 + \alpha_0^2 q^2)^2 \right. \\
& \left. + 2r_c^{3w+3} \left(-q^2(2\alpha_0^2 M r_c + r_c^4) + M r_c^2 (r_c^3 - 4\alpha_0^2 M) + \alpha_0^2 q^4 \right) \right)^2 \left. \right]. \tag{24}
\end{aligned}$$

Next, in Fig. 14, we have plotted the behaviour of $\tilde{\lambda}^2 - \kappa^2$ with respect to both the photon orbit radius r_c and the angular momentum L . Since, by definition, the chaos bound holds when $\tilde{\lambda}^2 - \kappa^2 < 0$ and is violated when $\tilde{\lambda}^2 - \kappa^2 > 0$, we find that for larger photon orbit radii the chaos bound is satisfied, and at smaller photon orbit radii it is violated, which implies that chaotic motion is more likely to be found in the near-horizon regime of the BH. Also, the bound holds at lower values of angular momentum and violates at higher values. This indicates that higher angular momentum photons tend to have chaotic orbits. Furthermore, the black hole parameters c , α_0 and q play important roles in the chaos bound. An increase in the value of c shifts the radius at which the bound is broken towards the horizon. The parameter α_0 and q also acts in a similar way shifting the critical radius where the bound is violated nearer to the horizon as they increase. In contrast, the critical value of angular momentum where the chaos bound is violated is very feebly affected by c values whereas α_0 and q does not practically affect the critical value of bound violation.

A. Scattering Cross Section

We finally determine the high-energy absorption cross-section through the Sinc approximation. Initially, Sanchez investigated the absorption cross-section for the Schwarzschild black hole in the UV regime and suggested that, as the frequency increases for a typical material sphere, the absorption cross-section grows monotonically while oscillating around the constant geometric-optics value associated with the black hole's photon sphere [80]. Next, the relationship between the impact parameter and the photon sphere's cross-section is established at critical values, thereby constraining the absorption cross-section. It follows that, at low energy scales, the absorption cross-section reflects the intrinsic properties of the black hole, matching its area, as shown by Das et al [81]. In contrast, at high energies, the geometric cross-section of the photon sphere can be examined using complex angular momentum methods [82], where Decanini et al. employed the Regge pole techniques to confirm that the high-energy absorption cross-section exhibits an oscillatory behaviour described by a $Sinc(x)$ function involving the photon sphere.

To calculate the total absorption cross section, one may use the Sinc approximation, which states that the total absorption cross section at the eikonal limit is given by $\sigma_{abs} \approx \sigma_{geo} + \sigma_{osc}$ [82], where σ_{geo} is the classical capture cross section of photon geodesics, which reduces from the total absorption cross section at the high fre-

quency limit. It is related to the critical impact parameter b_{crit} through $\sigma_{geo} = \pi b_{crit}^2$. Also, the oscillatory counterpart of the total cross section σ_{osc} at the eikonal limit can be given by:

$$\sigma_{osc} = -\frac{4\pi\tilde{\lambda}b_{crit}^2}{\omega} \exp(-\pi\tilde{\lambda}) \sin\left(\frac{2\pi\omega}{\Omega_{ph}}\right), \quad (25)$$

where $\tilde{\lambda}$ is the Lyapunov exponent, Ω_{ph} is the angular velocity at the critical orbit and r_{ph} is the radius of the photon sphere.

The total absorption cross section is plotted and shown in Fig. 15 (top panel). We can see that there is no drastic variation for different c values (when α_0 and q are kept fixed at 0.5 and 0.4 respectively) at the low frequency limit, but a slight variation is seen at high frequencies. Nevertheless, the variation is very negligible. Also, no variation is seen as l increases from 1 to 2. Next, concerning the values of α_0 parameter, shown in Fig. 15 (middle panel), the total absorption cross section increases with decreasing values of α_0 (when c and q are fixed at 0.0015 and 0.4 respectively). But, no effect is seen when l is increased from 1 to 2. Finally, the total absorption cross section is strongly influenced by the charge parameter q , where there is a visible effect on the amplitude of the total absorption cross section, as shown in Fig. 15 (bottom panel) It is seen that as the charge parameter decreases, the absorption cross section increases, irrespective of l values. In all the cases, however, a regular oscillation is maintained at the high frequency regime.

VII. CONCLUSION

In the first part, we analyzed the behavior of scalar quasinormal frequencies within the context of a Frolov BH in a quintessence field. We studied the quasinormal modes of the BH system by employing the first order WKB approximation to analyze how the Frolov BH coupled with the quintessence field dynamically responds to scalar perturbations. We have found that, with increasing values of c , the real part of the QNM frequency, drops, which corresponds to a decrease of the oscillatory behaviour of the spacetime as the intensity of the quintessence field increases. At the same time, an occurrence of less negative values of the QNM frequency in the imaginary counterpart, implying perturbations falling off more slowly. This suggests the effect of quintessence on the BH system's dynamical response against scalar perturbations.

We have also analyzed the dependence of greybody factors on the multipole moment l and black hole pa-

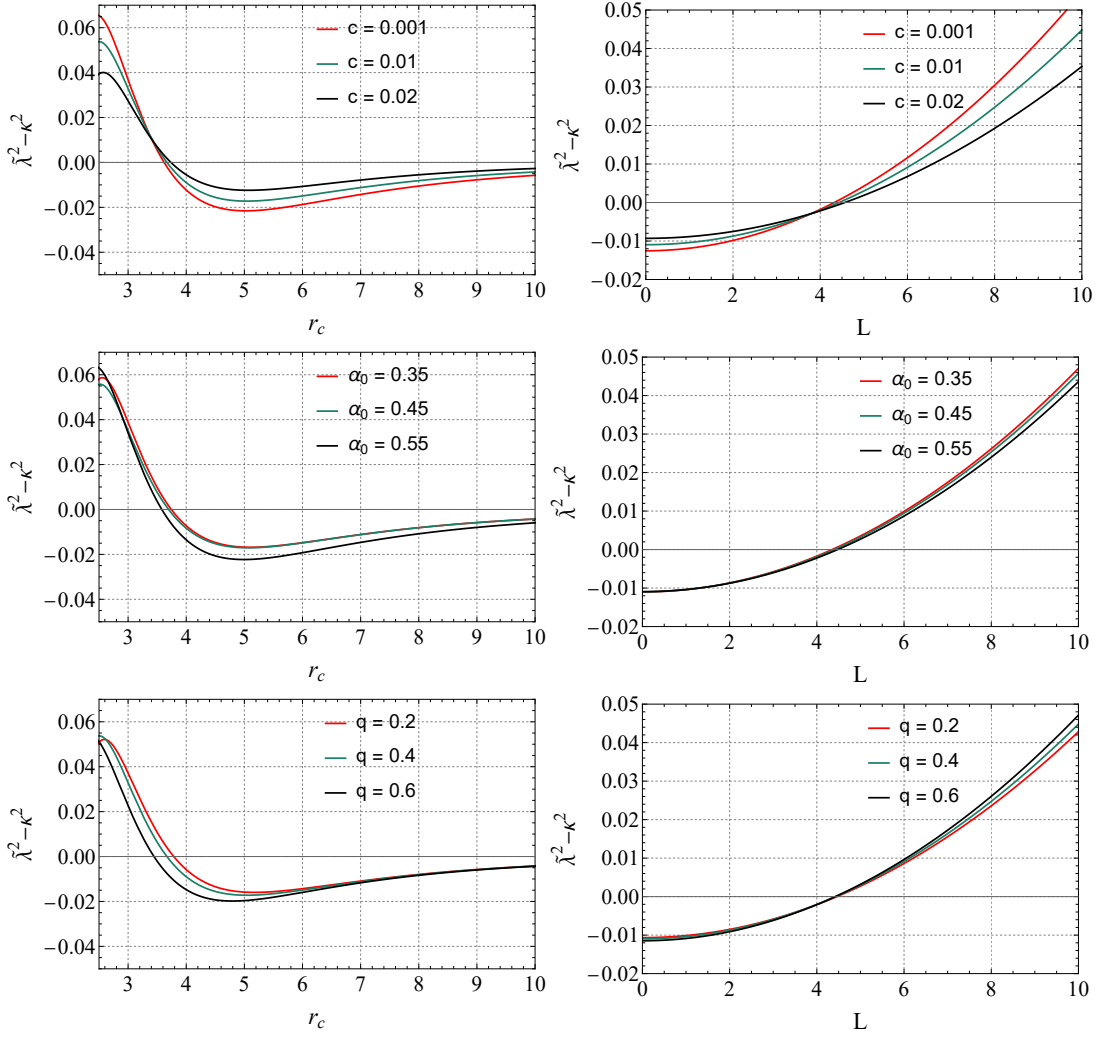


FIG. 14. The plot of chaos bound is shown for $w = -2/3$ for different values of c (top panel), α_0 (middle panel) and q (bottom panel).

rameters q , α_0 , and c . Lower multipole modes ($l = 1$) experience weaker barriers, enhancing transmission, while higher modes ($l = 2$) face stronger repulsion, reducing transmission efficiency. The charge q increases the barrier height, suppressing transmission, especially for higher l . The quintessence parameter c affects low-energy modes, while smaller α_0 steepens the barrier, reducing transmission. The transmission coefficient T_b shows strong sensitivity to q , further amplified for higher l , providing insights into wave propagation in modified black hole spacetimes.

We have studied the consequences of weak lensing around the BH system. The deflection angle of weak lensing α decreases monotonically with increasing impact parameter b , with a greater rate of decrease for larger c , indicating an enhanced repulsive effect from quintessence. In contrast, variations in α_0 and

q have negligible influence on α , as observed in the nearly unchanged deflection profiles. This suggests that the quintessence parameter c plays a dominant role in modifying light bending, while α_0 and q have minimal impact. The results highlight the significance of quintessence density in gravitational lensing effects around the black hole.

Finally, we analysed the chaos bound within the context of our BH systems. We find that, the chaos bound is satisfied for larger and violated for smaller radii of the circular photon orbits. This would in turn, imply that chaotic behaviour of photons in circular orbits is likely to manifest in the strong gravitational field nearer the BH. Moreover, the bound is obeyed for low angular momentum photons, while it is violated for high angular momentum photons. This suggests that high-angular-momentum photons are more likely to ex-

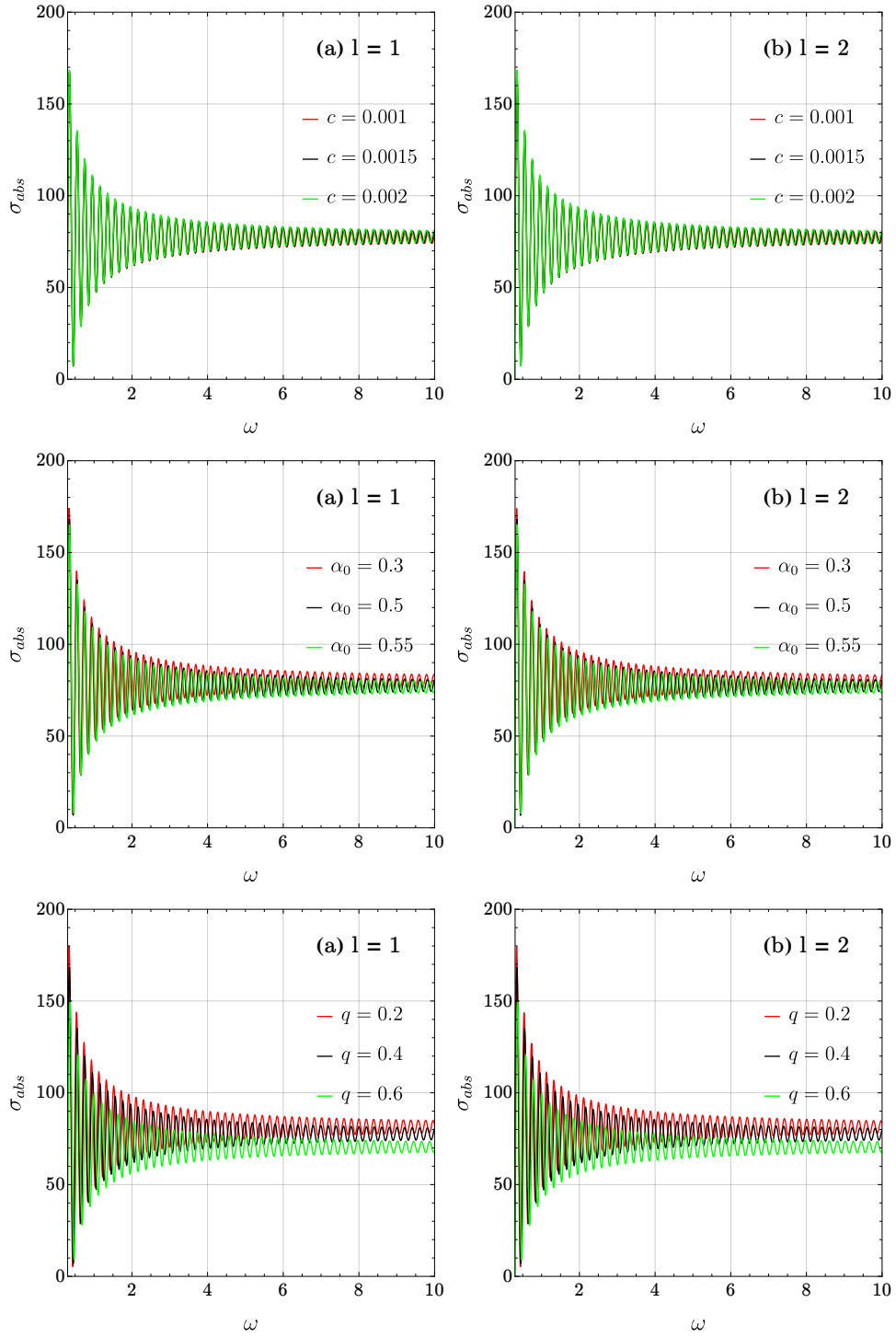


FIG. 15. The total absorption cross section is shown for different values of the model parameters and for different l values of the effective potential.

hibit chaotic trajectories. Physically, the violation of the chaos bound near the BH indicates that the quintessence field indeed has strong influence on its thermodynamic properties (as chaos bound is directly related to surface gravity, and hence temperature of the BH). These re-

sults suggest that some modifications may be feasible in the traditional framework of BH thermodynamics based on Bekenstein-Hawking entropy under the influence of quintessence. Then making use of the Lyapunov exponents, we also calculated the total absorption cross sec-

tion of radiation, which is intimately related to the critical photon orbit and impact parameter, which is found to be dependent mostly on the charge parameter and the Hubble length scale parameter, and depend mini-

mally on the quintessence parameter. The quintessence field however, seems to play a key role in the primary thermodynamic properties such as the BH temperature, possibly leading to potential deviations from standard GR predictions in the strong-field regime.

-
- [1] Event Horizon Telescope Collaboration, K. Akiyama, A. Alberdi, *et al.*, First Sagittarius A* Event Horizon Telescope Results. I. The Shadow of the Supermassive Black Hole in the Center of the Milky Way, *Astrophys. J. Lett.* **930**, L12 (2022).
- [2] V. P. Frolov, Notes on nonsingular models of black holes, *Phys. Rev. D* **94**, 104056 (2016).
- [3] Z. Song, H. Gong, H.-L. Li, *et al.*, Quasinormal modes and ringdown waveforms of a Frolov black hole, *Commun. Theor. Phys.* **76**, 105401 (2024).
- [4] R. Kumar, S. G. Ghosh, and A. Wang, Shadow cast and deflection of light by charged rotating regular black holes, *Phys. Rev. D* **100**, 124024 (2019).
- [5] J. Maldacena, The Large-N Limit of Superconformal Field Theories and Supergravity, *Int. J. Theor. Phys.* **38**, 1113 (1999).
- [6] D. T. Son and A. O. Starinets, Viscosity, Black Holes, and Quantum Field Theory, *Annu. Rev. Nucl. Part. Sci.* , **95** (2007).
- [7] A. Núñez and A. O. Starinets, AdS/CFT correspondence, quasinormal modes, and thermal correlators in $\mathcal{N} = 4$ supersymmetric Yang-Mills theory, *Phys. Rev. D* **67**, 124013 (2003).
- [8] D. Birmingham, I. Sachs, and S. N. Solodukhin, Conformal Field Theory Interpretation of Black Hole Quasinormal Modes, *Phys. Rev. Lett.* **88**, 151301 (2002).
- [9] T. Regge and J. A. Wheeler, Stability of a Schwarzschild Singularity, *Phys. Rev.* **108**, 1063 (1957).
- [10] F. J. Zerilli, Gravitational Field of a Particle Falling in a Schwarzschild Geometry Analyzed in Tensor Harmonics, *Phys. Rev. D* **2**, 2141 (1970).
- [11] F. J. Zerilli, Effective Potential for Even-Parity Regge-Wheeler Gravitational Perturbation Equations, *Phys. Rev. Lett.* **24**, 737 (1970).
- [12] C. V. Vishveshwara, Stability of the Schwarzschild Metric, *Phys. Rev. D* **1**, 2870 (1970).
- [13] C. V. Vishveshwara, Scattering of Gravitational Radiation by a Schwarzschild Black-hole, *Nature* **227**, 936 (1970).
- [14] C. Subrahmanyam and S. Detweiler, The quasi-normal modes of the Schwarzschild black hole, *Proc. R. Soc. Lond. A.* **344**, 441 (1975).
- [15] H.-J. Blome and B. Mashhoon, Quasi-normal oscillations of a schwarzschild black hole, *Phys. Lett. A* **100**, 231 (1984).
- [16] V. Ferrari and B. Mashhoon, New approach to the quasi-normal modes of a black hole, *Phys. Rev. D* **30**, 295 (1984).
- [17] E. W. Leaver, Solutions to a generalized spheroidal wave equation: Teukolsky's equations in general relativity, and the two-center problem in molecular quantum mechanics, *J. Math. Phys.* **27**, 1238 (1986).
- [18] E. W. Leaver, Spectral decomposition of the perturbation response of the Schwarzschild geometry, *Phys. Rev. D* **34**, 384 (1986).
- [19] W. Leaver E., An analytic representation for the quasinormal modes of Kerr black holes, *Proc. R. Soc. Lond. A.* **402**, 285 (1985).
- [20] G. T. Horowitz and V. E. Hubeny, Quasinormal modes of AdS black holes and the approach to thermal equilibrium, *Phys. Rev. D* **62**, 024027 (2000).
- [21] H. T. Cho, A. S. Cornell, J. Doukas, *et al.*, Black hole quasinormal modes using the asymptotic iteration method, *Classical Quantum Gravity* **27**, 155004 (2010).
- [22] E. Berti, V. Cardoso, and A. O. Starinets, Quasinormal modes of black holes and black branes, *Classical Quantum Gravity* **26**, 163001 (2009).
- [23] K. D. Kokkotas and B. G. Schmidt, Quasi-Normal Modes of Stars and Black Holes, *Living Rev. Relativ.* **2**, 2 (1999).
- [24] R. A. Konoplya and A. Zhidenko, Quasinormal modes of black holes: From astrophysics to string theory, *Rev. Mod. Phys.* **83**, 793 (2011).
- [25] E. Ayón-Beato and A. García, Regular Black Hole in General Relativity Coupled to Nonlinear Electrodynamics, *Phys. Rev. Lett.* **80**, 5056 (1998).
- [26] E. Ayon-Beato and A. Garcia, Non-Singular Charged Black Hole Solution for Non-Linear Source, *Gen. Relativ. Gravitation* **31**, 629 (1999).
- [27] E. Ayón-Beato and A. García, The Bardeen Model as a Nonlinear Magnetic Monopole, arXiv [10.1016/S0370-2693\(00\)01125-4](https://arxiv.org/abs/10.1016/S0370-2693(00)01125-4) (2000), gr-qc/0009077.
- [28] A. Flachi and J. P. S. Lemos, Quasinormal modes of regular black holes, *Phys. Rev. D* **87**, 024034 (2013).
- [29] B. Toshmatov, A. Abdujabbarov, Z. Stuchlík, *et al.*, Quasinormal modes of test fields around regular black holes, *Phys. Rev. D* **91**, 083008 (2015).
- [30] B. Toshmatov, Z. Stuchlík, and B. Ahmedov, Electromagnetic perturbations of black holes in general relativity coupled to nonlinear electrodynamics: Polar perturbations, *Phys. Rev. D* **98**, 085021 (2018).
- [31] L. A. López and V. Hinojosa, Quasinormal modes of charged regular black hole, *Can. J. Phys.* (2020).
- [32] J. Li, K. Lin, H. Wen, *et al.*, Gravitational Quasinormal Modes of Regular Phantom Black Hole, *Adv. High Energy Phys.* **2017**, 5234214 (2017).
- [33] C. Wu, Quasinormal frequencies of gravitational perturbation in regular black hole spacetimes, *Eur. Phys. J. C* **78**, 283 (2018).

- [34] *Regular Black Holes* (Springer Nature).
- [35] P. Bueno, P. A. Cano, and R. A. Hennigar, Regular Black Holes From Pure Gravity, arXiv [10.48550/arXiv.2403.04827](https://arxiv.org/abs/10.48550/arXiv.2403.04827) (2024), [2403.04827](https://arxiv.org/abs/2403.04827).
- [36] J. Maldacena, S. H. Shenker, and D. Stanford, A bound on chaos, *J. High Energy Phys.* **2016** (8), 106.
- [37] F. Pretorius and D. Khurana, Black hole mergers and unstable circular orbits, *Classical Quantum Gravity* **24**, S83 (2007).
- [38] N. J. Cornish and J. Levin, Lyapunov timescales and black hole binaries, *Classical Quantum Gravity* **20**, 1649 (2003).
- [39] V. Cardoso, A. S. Miranda, E. Berti, *et al.*, Geodesic stability, Lyapunov exponents and quasinormal modes, arXiv [10.1103/PhysRevD.79.064016](https://arxiv.org/abs/10.1103/PhysRevD.79.064016) (2008), [0812.1806](https://arxiv.org/abs/0812.1806).
- [40] S. Giri and H. Nandan, Stability analysis of geodesics and quasinormal modes of a dual stringy black hole via Lyapunov exponents, *Gen. Relativ. Gravitation* **53**, 76 (2021).
- [41] X. Lyu, J. Tao, and P. Wang, Probing the thermodynamics of charged Gauss Bonnet AdS black holes with the Lyapunov exponent, *Eur. Phys. J. C* **84**, 974 (2024).
- [42] F. Barzi, H. El Moumni, and K. Masmarr, Thermal chaos of charged-flat black hole via Rényi formalism, *Nucl. Phys. B* **1005**, 116606 (2024).
- [43] M. A. Saleem and A. Taani, The chaotic behavior of black holes: Investigating a topological retraction in anti-de Sitter spaces, *New Astron.* **107**, 102149 (2024).
- [44] I. S. Chowdhury, B. P. Akhouri, S. Haque, *et al.*, Simulating black hole quantum dynamics on an optical lattice using the complex Sachdev-Ye-Kitaev model, arXiv [10.48550/arXiv.2409.16553](https://arxiv.org/abs/10.48550/arXiv.2409.16553) (2024), [2409.16553](https://arxiv.org/abs/2409.16553).
- [45] J. Park and B. Gwak, Bound on Lyapunov exponent in Kerr-Newman-de Sitter black holes by a charged particle, *J. High Energy Phys.* **2024**, 23.
- [46] Y.-Q. Lei, X.-H. Ge, and C. Ran, Chaos of particle motion near a black hole with quasitopological electromagnetism, *Phys. Rev. D* **104**, 046020 (2021).
- [47] B. Singh, N. Padhi, and R. R. Nayak, Circular orbits and chaos bound in slow-rotating curved acoustic black holes, arXiv [10.48550/arXiv.2405.12337](https://arxiv.org/abs/10.48550/arXiv.2405.12337) (2024), [2405.12337](https://arxiv.org/abs/2405.12337).
- [48] Y.-Q. Lei, X.-H. Ge, and S. Dalui, Thermodynamic Stability Versus Chaos Bound Violation in D-dimensional RN Black Holes: Angular Momentum Effects and Phase Transitions, arXiv [10.1016/j.physletb.2024.138929](https://arxiv.org/abs/10.1016/j.physletb.2024.138929) (2024), [2404.18193](https://arxiv.org/abs/2404.18193).
- [49] H.-L. Li, B.-Q. Zhang, X.-M. Jiao, *et al.*, Mutual correlation and chaotic behavior in phantom AdS black holes in both dynamic and static backgrounds, *Results Phys.* **64**, 107895 (2024).
- [50] H. L. Prihadi, F. P. Zen, D. Dwiputra, *et al.*, Localized chaos due to rotating shock waves in Kerr-AdS black holes and their ultraspinning version, *Gen. Relativ. Gravitation* **56**, 90 (2024).
- [51] J. Lu and X. Wu, Effects of Two Quantum Correction Parameters on Chaotic Dynamics of Particles near Renormalized Group Improved Schwarzschild Black Holes, *Universe* **10**, 277 (2024).
- [52] A. N. Kumara, S. Punacha, and M. S. Ali, Lyapunov Exponents and Phase Structure of Lifshitz and Hyperscaling Violating Black Holes, arXiv [10.48550/arXiv.2401.05181](https://arxiv.org/abs/10.48550/arXiv.2401.05181) (2024), [2401.05181](https://arxiv.org/abs/2401.05181).
- [53] S. A. Hayward, Formation and Evaporation of Nonsingular Black Holes, *Phys. Rev. Lett.* **96**, 031103 (2006).
- [54] V. V. Kiselev, Quintessence and black holes, *Classical Quantum Gravity* **20**, 1187 (2003).
- [55] M. M. Gohain, K. Bhuyan, R. Borgohain, *et al.*, Frolov Black Hole Surrounded by Quintessence – I: Thermodynamics, Geodesics and Shadows, arXiv [10.48550/arXiv.2412.06252](https://arxiv.org/abs/10.48550/arXiv.2412.06252) (2024), [2412.06252](https://arxiv.org/abs/2412.06252).
- [56] X.-X. Zeng and H.-Q. Zhang, Influence of quintessence dark energy on the shadow of black hole, *Eur. Phys. J. C* **80**, 1058 (2020).
- [57] G. Mustafa, F. Atamurotov, I. Hussain, *et al.*, Shadows and gravitational weak lensing by the Schwarzschild black hole in the string cloud background with quintessential field*, *Chin. Phys. C* **46**, 125107 (2022).
- [58] A. Belhaj, M. Benali, A. E. Balali, *et al.*, Deflection angle and shadow behaviors of quintessential black holes in arbitrary dimensions, *Classical Quantum Gravity* **37**, 215004 (2020).
- [59] H. Chen, B. C. Lütfüoğlu, H. Hassanabadi, *et al.*, Thermodynamics of the Reissner-Nordström black hole with quintessence matter on the EGUP framework, *Phys. Lett. B* **827**, 136994 (2022).
- [60] B. Toshmatov, Z. Stuchlík, and B. Ahmedov, Rotating black hole solutions with quintessential energy, *Eur. Phys. J. Plus* **132**, 98 (2017).
- [61] S. Fernando and J. Correa, Quasinormal modes of the Bardeen black hole: Scalar perturbations, *Phys. Rev. D* **86**, 064039 (2012).
- [62] K. Jusufi, Quasinormal modes of black holes surrounded by dark matter and their connection with the shadow radius, *Phys. Rev. D* **101**, 084055 (2020).
- [63] B. F. Schutz and C. M. Will, Black hole normal modes - A semianalytic approach, *Astrophys. J.* **291**, L33 (1985).
- [64] N. Zettili, *Quantum Mechanics: Concepts and Applications, 3rd Edition* (2022).
- [65] D. J. Griffiths and D. F. Schroeter, *Introduction to Quantum Mechanics* (2018).
- [66] S. Iyer, Black-hole normal modes: A WKB approach. II. Schwarzschild black holes, *Phys. Rev. D* **35**, 3632 (1987).
- [67] S. Iyer and C. M. Will, Black-hole normal modes: A WKB approach. I. Foundations and application of a higher-order WKB analysis of potential-barrier scattering, *Phys. Rev. D* **35**, 3621 (1987).
- [68] R. A. Konoplya, Quasinormal behavior of the D-dimensional Schwarzschild black hole and the higher order WKB approach, *Phys. Rev. D* **68**, 024018 (2003).
- [69] R. A. Konoplya, Quasinormal modes in higher-derivative gravity: Testing the black hole parametrization and sensitivity of overtones, *Phys. Rev. D* **107**, 064039 (2023).
- [70] R. A. Konoplya, A. Zhidenko, and A. F. Zinhailo, Higher order WKB formula for quasinormal modes and greybody factors: recipes for quick and accurate calculations, *Classical Quantum Gravity* **36**, 155002 (2019).

- [71] S. W. Hawking, Particle creation by black holes, *Commun. Math. Phys.* **43**, 199 (1975).
- [72] D. Singleton and S. Wilburn, Hawking Radiation, Unruh Radiation, and the Equivalence Principle, *Phys. Rev. Lett.* **107**, 081102 (2011).
- [73] V. Akhmedova, T. Pilling, A. de Gill, *et al.*, Temporal contribution to gravitational WKB-like calculations, *Phys. Lett. B* **666**, 269 (2008).
- [74] J. Maldacena and A. Strominger, Black hole greybody factors and D-brane spectroscopy, *Phys. Rev. D* **55**, 861 (1997).
- [75] M. Cvetič and F. Larsen, General rotating black holes in string theory: Greybody factors and event horizons, *Phys. Rev. D* **56**, 4994 (1997).
- [76] M. Visser, Some general bounds for one-dimensional scattering, *Phys. Rev. A* **59**, 427 (1999).
- [77] P. Boonserm and M. Visser, Bounding the Bogoliubov coefficients, *Ann. Phys.* **323**, 2779 (2008).
- [78] A. Ishihara, Y. Suzuki, T. Ono, *et al.*, Gravitational bending angle of light for finite distance and the Gauss-Bonnet theorem, *Phys. Rev. D* **94**, 084015 (2016).
- [79] P. Su and C.-K. Qiao, Gravitational Lensing of Euler-Heisenberg Black Hole Surrounded by Perfect Fluid Dark Matter, arXiv: 2410.02411 [gr-qc] [10.48550/arXiv.2410.02411](https://arxiv.org/abs/2410.02411) (2024), [2410.02411](https://arxiv.org/abs/2410.02411).
- [80] N. Sanchez, Absorption and emission spectra of a Schwarzschild black hole, *Phys. Rev. D* **18**, 1030 (1978).
- [81] S. R. Das, G. Gibbons, and S. D. Mathur, Universality of Low Energy Absorption Cross Sections for Black Holes, *Phys. Rev. Lett.* **78**, 417 (1997).
- [82] Y. Décanini, G. Esposito-Farèse, and A. Folacci, Universality of high-energy absorption cross sections for black holes, *Phys. Rev. D* **83**, 044032 (2011).